Biochimica et Biophysica Acta 1798 (2010) 1503–1511

Contents lists available at ScienceDirect

Biochimica et Biophysica Acta

journal homepage: www.elsevier.com/locate/bbamem

Specific anchoring modes of two distinct dystrophin rod sub-domains interacting in phospholipid Langmuir films studied by atomic force microscopy and PM-IRRAS

V. Vié [a,*], S. Legardinier [b], L. Chieze [a], O. Le Bihan [a], Y. Qin [a], J. Sarkis [a,b], J.-F. Hubert [b], A. Renault [a], B. Desbat [c], E. Le Rumeur [b]

[a] Université de Rennes 1, Institut de Physique UMR CNRS 6251, Rennes, France
[b] Université de Rennes 1, UMR CNRS 6026, IFR140, Rennes, France
[c] Université de Bordeaux 1, CBMN UMR CNRS 5248, ENITAB, 33607 Pessac, France

ARTICLE INFO

Article history:
Received 3 November 2009
Received in revised form 2 April 2010
Accepted 7 April 2010
Available online 14 April 2010

Keywords:
Dystrophin rod domain
Spectrin-like repeats
Langmuir films
Atomic force microscopy
Polarization modulation infrared spectroscopy

ABSTRACT

Dystrophin rod repeats 1–3 sub-domain binds to acidic phosphatidylserine in a small vesicle binding assay, while the repeats 20–24 sub-domain does not. In the present work, we studied the adsorption behaviour of both sub-domains at the air/liquid interface and at the air/lipid interface in a Langmuir trough in order to highlight differences in interfacial properties. The adsorption behaviour of the two proteins at the air/liquid interface shows that they display surface activity while maintaining their alpha-helical secondary structure as shown by PM-IRRAS. Strikingly, R20–24 needs to be highly hydrated even at the interface, while this is not the case for R1–3, indicating that the surface activity is dramatically higher for R1–3 than R20–24. Surface-pressure measurements, atomic force microscopy and PM-IRRAS are used in a Langmuir experiment with DOPC–DOPS monolayers at two different surface pressures, 20 mN/m and 30 mN/m. At the lower surface pressure, the proteins are adsorbed at the lipid film interface while maintaining its alpha-helical structure. After an increase of the surface pressure, R1–3 subsequently produces a stable film, while R20–24 induces a reorganization of the lipid film with a subsequent decrease of the surface pressure close to the initial value. AFM and PM-IRRAS show that R1–3 is present in high amounts at the interface, being arranged in clusters representing 3.3% of the surface at low pressure. By contrast, R20–24 is present at the interface in small amounts bound only by a few electrostatic residues to the lipid film while the major part of the molecule remains floating in the sub-phase. Then for R1–3, the electrostatic interaction between the proteins and the film is enhanced by hydrophobic interactions. At higher surface pressure, the number of protein clusters increases and becomes closer in both cases implying the electrostatic character of the binding. These results indicate that even if the repeats exhibit large structural similarities, their interfacial properties are highly contrasted by their differential anchor mode in the membrane. Our work provides strong support for distinct physiological roles for the spectrin-like repeats and may partly explain the effects of therapeutic replacement of dystrophin deficiency by minidystrophins.

1. Introduction

Dystrophin is a large filamentous cytoskeletal protein of the muscle and nerve cells, localized along the internal face of the sarcolemma [1,2]. It forms an array of filaments interacting with both cytoskeletal actin and plasma membrane, via interaction with a complex of intrinsic membrane proteins [for review, see [3]]. Interactions with membrane have also been suggested by *in vitro* studies showing that specific parts of the central rod domain interact with anionic and/or zwitterionic phospholipids [4–6]. These interactions, while not yet demonstrated to be involved in a cellular environment, may be a key feature in controlling resistance to the stress of contraction–relaxation cycles in muscle cells. In the absence of dystrophin due to dystrophin gene mutations, sarcolemma ruptures are frequent and lead to cellular leakage which therefore speeds up muscle degeneration, one of the major physio-pathological processes of muscular dystrophies [7–9].

Dystrophin rod domain is made up of 24 homologous spectrin-like repeats of about 110 residues, structured in three helix coiled-coils, which could be considered as a series of three sub-domains separated by hinges, i.e. repeats 1 to 3, repeats 4 to 19 and repeats 20 to 24 [10,11].

We focused our study on repeats 1 to 3 (R1–3) and repeats 20 to 24 (R20–24) sub-domains. The first is localized close to N-terminal end which is known to be an actin domain binding while R20–24 is placed close to the C-terminal end that links to the membrane dystroglycan complex.

Abbreviations: AFM, atomic force microscopy; LB film, Langmuir–Blodgett film; PM-IRRAS, polarization modulated-infrared reflection–absorption spectroscopy

* Corresponding author. Institut de Physique de Rennes, Bât. 11, Campus Beaulieu, l Université Rennes 1, France. Tel.: +33 2 23 23 56 45; fax: +33 2 23 23 67 17.
E-mail address: veronique.vie@univ-rennes1.fr (V. Vié).

0005-2736/$ – see front matter © 2010 Elsevier B.V. All rights reserved.
doi:10.1016/j.bbamem.2010.04.005

In a previous work, we studied the phospholipid-binding properties of the dystrophin rod domain [5,6] using small vesicles showing that R1–3 displays phospholipid-binding properties while on the contrary, the R20–24 sub-domain does not display such properties [12]. Electrostatic forces as well as hydrophobic forces likely contribute to the binding of the R1–3 sub-domain to anionic phospholipid vesicles, leading to the formation of stable phospholipid–protein complexes which can be separated by exclusion chromatography.

However, determining the relationship of structure to function requires following the potential trans-conformation of proteins upon binding to phospholipid as well as the influence of the protein upon the lipid interfacial properties. This could be achieved by changing the membrane model, which would involve switching from the small vesicle bilayer system to monolayer films [13]. Due to their amphiphilic structure, phospholipids form a two-dimension monolayer on the liquid surface, as in a Langmuir trough, and therefore resemble half of the membrane bilayer. Their molecular arrangement can be controlled by changing temperature and molecular area, as well as sub-phase and surface pressure as previously shown with spectrin, a molecule of the same family as dystrophin [14,15]. Several techniques associated with the Langmuir trough provide information about the protein and the lipid interfacial arrangements, including surface-pressure measurement, polarization modulated-infrared reflection absorption spectroscopy (PM-IRRAS) [16,17] and atomic force microscopy (AFM) [18]. These methods are particularly well suited for studying interfacial proteins which interact with biological membranes. We have previously used these methods to improve our understanding of protein–lipid interactions of the wheat protein puroindolines [19,20]. By varying parameters such as the surface pressure in order to change the density of the lipid head-groups and the charge density, it is possible to modulate the protein interaction with lipids. It is known that electrostatic interactions are favoured by a strong surface pressure, while hydrophobic interactions are facilitated by lower surface pressure. In this study, we use this modulation approach to investigate the interfacial air/liquid and lipid/liquid properties of dystrophin sub-domain R1–3 and R20–24. We show that the R1–3 domain has a very high activity with respect to anionic phospholipid films, which allows a partial insertion of the protein, at low surface pressure, into the monolayer via hydrophobic forces. On the other hand, the R20–24 domain appears to be adsorbed at the interface solely by electrostatic forces, but only via a few residues. Understanding the potential value of the therapeutic replacement of dystrophin with mini- or micro-dystrophins requires a complete structural and functional characterization of the protein domains, including the molecular mechanisms of their interactions with lipids or proteins. Our results stress that even though these repeats share large sequence homology, they display quite different physico-chemical properties, indicating that they may have different roles in the muscle cell and that a sub-set of the repeats may be present in therapeutic molecules.

2. Materials and methods

2.1. Materials

1,2-Dioleyl-sn-glycero-3-phosphocholine (DOPC) and 1,2-dioleyl-sn-glycero-3-phosphoserine (DOPS) were purchased from Avanti Polar Lipids (Alabama, US), and were used without further purification.

2.2. Preparations of recombinant dystrophin rod domain proteins

The recombinant proteins (Table 1) were expressed in *E. coli*. Isolation and purification of the GST-proteins R1–3 ad R20–24 used in these experiments have been described previously [12]. The glutathion-4B-sepharose bound GST-proteins were eluted after on-column thrombin cleavage for 48 h at 4 °C in 10 mM Tris (pH 7.5) and 150 mM NaCl, 1 mM EDTA (TNE buffer). Proteins were eventually further purified on ion-exchange chromatography columns from HiTrap™ IEX Selection Kit and quantified using the BCA (bicinchoninic acid) protein assay.

Table 1
Human dystrophin rod domain constructs.

Construct (number of residue)	Start and end residues	N-terminus	C-terminus
R1–3 (333)	338–668	*GS*(S)**E**VNLD…	…KSTAQISQ**A**
R20–24 (574)	2469–3040	*GS***V**PALA…	…VRQLH**E**

*Construct of DeWolf et al. [4].
Residue in bold is the start (N-terminus column) or end (C-terminus column) residue of the repeat from the Winder alignment [11].
GS in smaller characters and italics indicates the two residues left at the N-terminus after thrombin cleavage of the GST-tag.

2.3. Monolayer measurements

The surface pressure (π) was measured with a filter paper held by a Wilhelmy balance connected to a microelectronic feedback system ($\pi = \gamma_0 - \gamma$, where γ_0 and γ were, respectively, the surface tension value without or with presence of molecules at the air/liquid interface). Before starting the experiments, the trough was cleaned with chloroform, ethanol and water, and then filled up with TNE buffer. The air/liquid interface was cleaned from impurities by repeated aspiration and filling. Each experiment was started when the fluctuation of the surface pressure was lower than 0.2 mN/m during the compression.

2.3.1. Air/liquid interface measurements

A small circular Teflon trough containing a sub-phase volume of 4 or 8 mL was used and filled with TNE buffer. The protein was then injected from a 50 µM stock solution into the sub-phase solution through a hole in the trough using a microsyringe. The final protein concentration ranged from 4.10^{-8} to 100.10^{-8} M. The surface pressure recordings started at the moment of protein injection into the sub-phase and continued for a further 7 h after surface pressure stabilization. Each experiment was repeated at least three times. The reproducibility of π values was estimated at ±0.5 mN/m.

2.3.2. Lipid/liquid interface measurements

Computer-controlled and user-programmable Langmuir troughs (Nima Technology, Cambridge, UK) equipped with two movable barriers were used for surface pressure-measurements, AFM sample preparations and PM-IRRAS experiments. Lipid mixture (DOPC/DOPS (1:1, M:M)) or pure DOPC or DOPS in chloroform/methanol 2:1 (v/v) was gently deposited at the air/liquid interface of the TNE buffer sub-phase. After 10 min to allow evaporation of the solvent, lipid films were compressed by moving barriers at a rate of 20 cm²/min or 8 cm²/min in function of the trough size (700 cm² or 70 cm², respectively) and equilibrated at the desired surface pressure (from 20 to 30 mN/m). Then, the protein was injected into the sub-phase just beneath the lipid monolayer. The increase of surface pressure due to adsorption of the protein onto the monolayer was recorded continuously as a function of time. Experiments were conducted at room temperature.

2.4. Atomic force microscopy

AFM imaging of Langmuir–Blodgett films (LB films) was performed in contact mode using a Pico-plus atomic force microscope (Agilent Technologies, Phoenix, AZ) under ambient conditions with a scanner of 10×10 µm². Topographic images were acquired in

constant force mode using silicon nitride tips on integral cantilevers with a nominal spring constant of 0.06 N/m. Samples for imaging were obtained using the Langmuir–Blodgett technique from Langmuir films. After stabilization of the surface pressure, the Langmuir film was transferred onto freshly cleaved mica plates at constant surface pressure by raising the mica vertically (at 1 mm/min) through the lipid/liquid interface. Images were obtained from at least two samples prepared on different days with at least five macroscopically separated areas on each sample.

2.4.1. Analysis of the shape of protein clusters on the AFM images

AFM images of 5×5 μm² size were analysed to characterize the protein clusters. For these images, the height resolution is 0.078 nm (Z-range = 20 nm; 256 grey levels). Images were exported from the AFM microscope in TIFF format, at a resolution of 24 bits and with a size of 512×512 pixels. The images were analysed with ImageJ. To determine the position of the centre, area and height of objects in the AFM images, we performed the following procedure. All images were similarly thresholded. The pixels with a grey level above the threshold were given the value 255, while the others were given a null value. Therefore, in the binarized images, we could calculate the number, the position of the centre and the area of the objects. Then, the program searched on the grey-level images for the maximal grey value around the centre of the object to determine its height.

2.5. Polarization modulated-infrared reflection–absorption spectroscopy (PM-IRRAS)

The PM-IRRAS spectra were recorded on a Nicolet (Thermo Electron, Madison, WI) 870 FT-IR spectrometer. The FT is calculated with data points every 1 cm^{-1} with a final spectral resolution of 8 cm^{-1} by co-adding 600 scans (corresponding to an acquisition time of 10 min) at different surface pressures. In these experiments, intrinsic peak widths are no lower than 25 cm^{-1}, so a spectral resolution of 8 cm^{-1} represents the minimum wavelength number difference required to discriminate accurately the presence of distinct peaks. The details of the optical setup, the experimental procedure and the two-channel processing of the detected intensity have been already described [16]. Langmuir films of protein at the air/liquid or liquid/lipid interfaces were formed on 8 mL or 60 mL Langmuir troughs, respectively, as described above. The PM-IRRAS spectra were acquired at several times during the stabilization of the surface pressure, and then displayed after subtraction of the water bands from the sub-phase (TNE buffer) spectrum or subtraction of the lipid spectrum (this is noted in the legends). They were recorded from 4000 to 940 cm^{-1}. Between 3000 and 2600 cm^{-1}, two bands are associated to the anti-symmetric and symmetric CH_2 stretching mode of lipid acyl chains. In the region from 1850 cm^{-1} to 1250 cm^{-1}, there appear the two amide I and amide II bands of the proteins and several bands of the lipid head-groups (detailed in Results section).

The analysis of PM-IRRAS spectra in terms of molecular orientation relative to the interface relies on a specific surface selection rule. The intensity and the positive or negative orientation of the IR bands relative to the interface are correlated with the transition moments [21]. In particular, the simulated PM-IRRAS spectra of the amide I and II bands for an α-helix peptide with different orientations in the film show that the ratio between the intensities of amide I and amide II bands RI/II, is dependent on the tilt angle θ of the helix with respect to the normal to the interface [21–23]. It is worth to note that dystrophin is a large filamentous protein and that the sub-domains studied here are composed of five (R20–24) or three (R1–3) repeats, each constituted by three helices structured in coiled-coil. Then the helices should be essentially parallel in a repeat and the repeats in each sub-domain are more or less in the same plane.

Experiments are conducting on different days with two batches of protein purification.

3. Results

Before investigating the properties of dystrophin repeats in interaction with lipids in the monolayer, characterization of the protein properties at the air/liquid interface was performed. This is done firstly to determine the concentration to be used to avoid a potential aggregation of protein in the solution and secondly, to establish the protein saturation of the interface. Furthermore, PM-IRRAS is used to detect the modifications of protein conformation.

3.1. The amphiphilic character of both proteins promotes their absorption without drastic structural changes

Adsorption of the two proteins at the air/liquid interface was studied using surface pressure, and PM-IRRAS.

3.1.1. Effect of protein concentration on surface pressure at the air/liquid interface

Proteins dissolved in TNE buffer were injected into the sub-phase of a 4 mL trough filled with the same buffer in the range 4.10^{-8} to 100.10^{-8} M. For each concentration, the kinetic of the protein absorption was followed by recording the surface pressure. The maximal surface pressure or final surface pressure reached at the equilibrium ("pseudo equilibrium") protein adsorption is noted. Fig. 1A reports the variations of the final surface pressures according to the protein concentration in bulk. It can be observed that increasing concentrations of both proteins led to a progressively greater interfacial pressure until maximal values of 20.4 and 19.7 mN/m observed for R1–3 and R20–24, respectively. Above a protein concentration of 20.10^{-8} M surface pressures were effectively constant. These results show that the proteins display a pronounced surface activity. The beginning of this plateau is observed at a protein concentration of $16.6.10^{-8}$ M then this concentration was sufficiently low to avoid potential aggregation of proteins in the sub-phase and it was adopted for further experiments.

3.1.2. PM-IRRAS spectroscopy

Possible changes in conformation and orientation of the two proteins at the air/liquid interface were examined using polarization modulated-infrared absorption–reflection spectroscopy (Fig. 1B and C). Spectra were acquired immediately after the protein injection at the bulk concentration of $16.6.10^{-8}$ M, when the surface pressure started to increase, at the beginning of the plateau (only for R20–24) and after complete stabilization of the surface pressure at 18.5 mN/m and 18.7 mN/m for R20–24 and R1–3 respectively.

A general inspection of the graphs indicates the presence of two specific bands centred at 1653 cm^{-1} and 1545 cm^{-1} attributed to the amide I and amide II signals, respectively.

As regards R20–24 (Fig. 1B), in the first spectrum acquired just after the protein injection, the amide I region is strongly distorted by the presence of a negative band appearing between 1500 and 1700 cm^{-1} with a very weak maximum at 1655 cm^{-1}. This behaviour has been previously observed and calculated for a highly hydrated protein monolayer at the interface [24]. In this condition, the amide bands are very broad and their intensities sometimes decrease by one order of magnitude. First of all, the amide I peak is very broad and the spectra show shoulders characteristics of turns and random structure (~1675 and ~1640 cm^{-1}) in addition to the alpha-helix structure. The amide I signal increases and remains stable during stabilization of the surface pressure at 18.5 mN/m. In contrast to amide I, the amide II band increases during the kinetic experiment. Therefore, during the adsorption, there is an increase of matter at the interface as well as a reorientation. We previously showed that it is possible to use the amide I/II intensity ratio, RI/II, to determine the average angle with respect to the normal to the monolayer between the protein and the interface [25]. Here, the very high value of $R_{I/II}$ indicates an alpha-

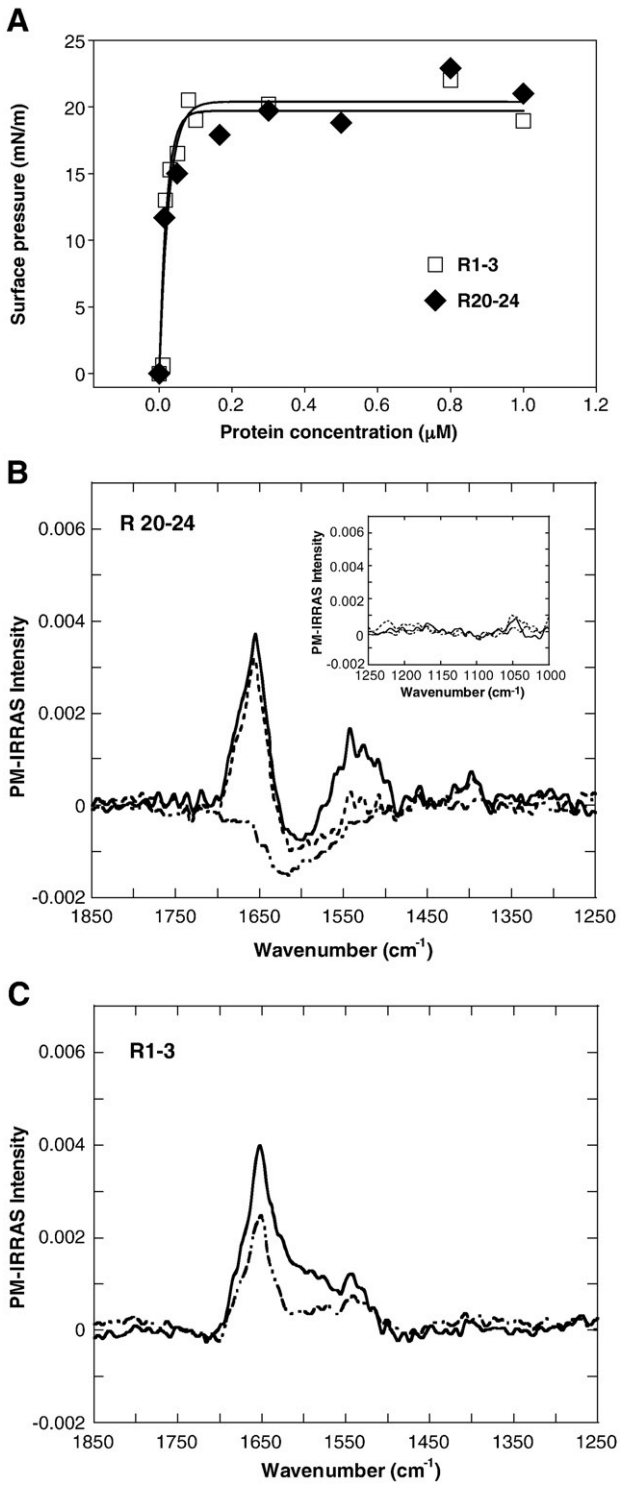

Fig. 1. Absorption of proteins at the air/liquid interface. (A) Final surface pressure reached at the end of the adsorption kinetic experiment as a function of the protein sub-phase concentration in a Langmuir trough. Each point corresponds to the mean value of three kinetic experiments. (B, C) PM-IRRAS spectra acquired during protein adsorption at the air/liquid interface of R20–24 (B) and R1–3 (C). Spectra are acquired at the initial surface pressure (dash–dot–dot), at the beginning of the surface pressure plateau (short dash) and after stabilization of the surface pressure (solid line). The insert in B shows the region between 1000 and 1150 cm^{-1} for R20–24. The protein concentrations on the sub-phase are 0.166 μM.

helical arrangement rather parallel to the air/liquid interface at the beginning of the plateau. Later, the ratio decreases and becomes close to 2.75 (i.e. the amide II band increases faster than the amide I band), indicating an average angle of 57° with respect to the normal at the air/liquid interface. Two peaks were observed, located at 1397 cm^{-1} and 1050 cm^{-1}, having similar intensity specifically for R20–24 (Fig. 1B insert). A spectrum of the buffer was recorded using ATR (spectra not shown here), which showed the same peak positions, indicating that R20–24 promotes a higher local concentration or induces a specific orientation of Tris molecules at the interface.

The spectra recorded from R1–3 are quite different from those obtained from R20–24. The amide I and II bands remain very sharp throughout the experiment and there is no evidence of recruitment or reorientation of Tris molecules. Two spectra from R1–3 were recorded at the beginning and after stabilization of the surface pressure at 18.7 mN/m (Fig. 1C). In the first spectrum, the amide I and amide II bands appear with a maximum wavenumber located at 1653 and 1545 cm^{-1}, respectively, mainly reflecting a high content of α-helix protein structure. After stabilization of the surface pressure, the intensity of the two peaks increases, indicating an increase of matter at the air/liquid interface. During the same time, RI/II remains at a value of 3.2, which yields an average angle of 61° of the protein with respect to the normal of the monolayer. Therefore, it appears that the protein moves to the interface without further reorientation. In the region situated between the two amide I and II bands, the signal increases to form a shoulder around 1600 cm^{-1}. Such a spectrum shape could be due to the modification of the optical indices of the buffer, or more likely, the presence of N–H bending mode due to the very high number of lysine, arginine, glutamic and aspartic acid residues [26] which account for 99 over the 333 total residues.

Overall, these results show that the proteins remain structured in α-helices as previously shown by circular dichroism [12].

3.2. The two sub-domains behave very differently in contact with lipid monolayers

Previous data have shown that R1–3 interacts with DOPC/DOPS small vesicles forming a stable lipid/protein complex isolated by exclusion chromatography. In contrast any stable lipid/protein complex is detected between R20–24 and these small vesicles [12]. Moreover, none of the proteins bind to PC/PE vesicles. Therefore, in this study, we attempt to further characterize the interaction with anionic lipids (DOPS). The lipid mixture is essentially DOPC/DOPS 1:1 nevertheless additional experiment with each pure lipid was performed for R1–3. Evaluation of the adsorption was carried out using atomic force microscopy (AFM) and PM-IRRAS.

3.2.1. Effect of protein injection on surface pressure of lipid film

The lipid mixture was spread at the interface Langmuir trough to form a monolayer. After compression and stabilization of the lipid film to 20 mN/m the proteins dissolved in TNE buffer were injected into the sub-phase while the surface pressure was continuously monitored (Fig. S1 in the Supplementary material). R1–3 induced a progressive increase to a stable plateau at 27 mN/m. By contrast, R20–24 induced a first increase to 25 mN/m, but later on the surface pressure declined progressively to a lower value of 21 mN/m. For the initial lipid surface pressure of 30 mN/m, no modification of the surface pressure is measured after proteins injection.

3.2.2. Atomic force microscopy and image analysis

Atomic force microscopy images were acquired on transferred lipid and protein/lipid films using the Langmuir–Blodgett technique. For both proteins, transfer for AFM was done at the end of the adsorption kinetic for the two initial surface pressures of 20 and 30 mN/m. The images obtained for DOPC/DOPS 1:1 films at 20 mN/m and at 30 mN/m without protein are presented in Fig. 2, A and B respectively. These images show a flat surface without defects. The protein/lipid film displayed in Fig. 2C to 2F appears as a homogeneous dark flat background dotted with isolated white protrusions.

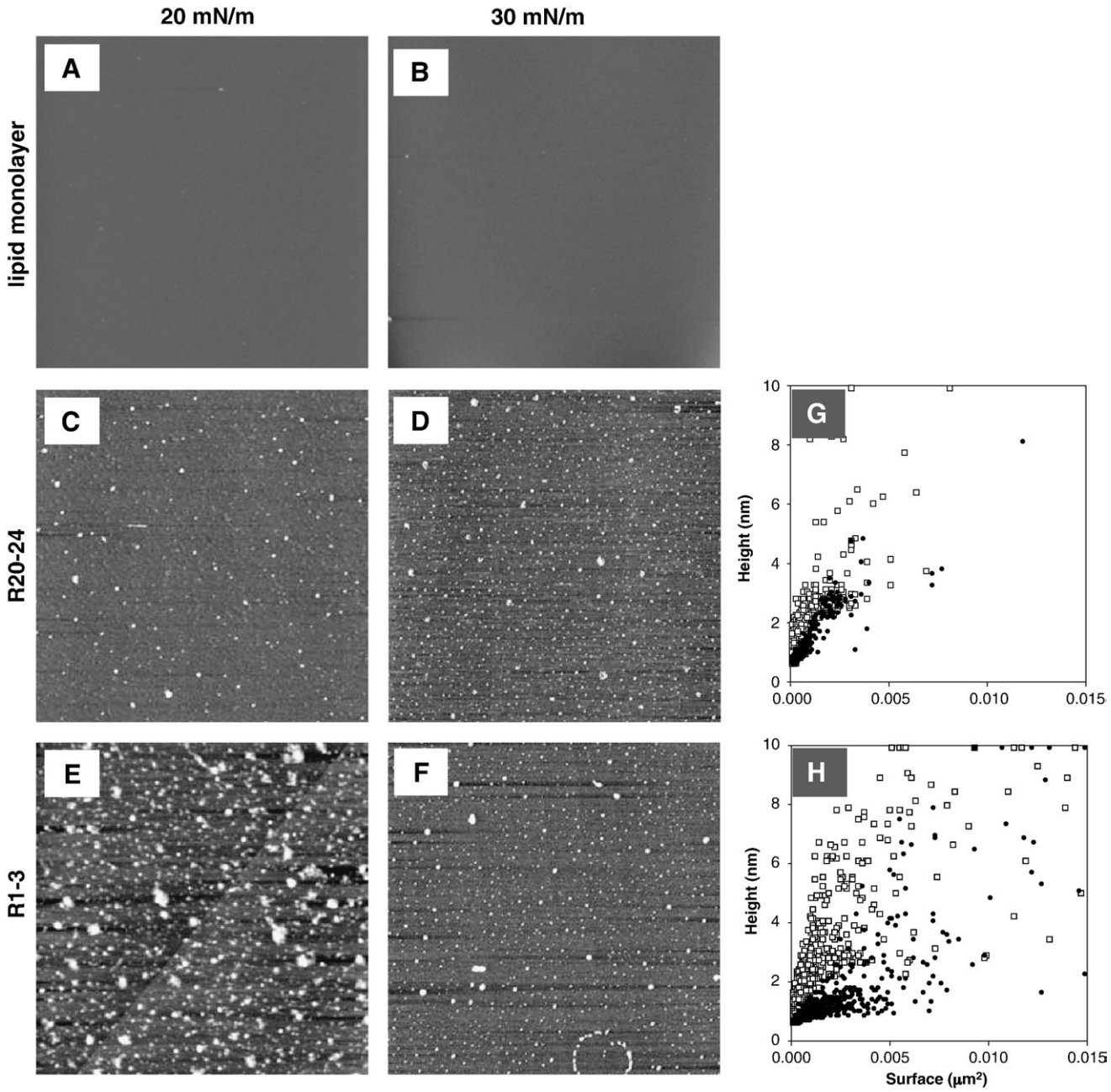

Fig. 2. AFM images of transferred monolayers. A and B correspond to the DOPC/DOPS 1:1 monolayer at 20 and 30 mM/m respectively. C–F are obtained imaging the transferred protein/lipid films for protein absorption onto lipid films at an initial pressure of 20 (C and E to B) or 30 (D and F to D) mN/m for R20–24 (C and D), and R1–3 (E and F). The scan size is 5 μm × 5 μm. Grey scale: *z*-range is 10 nm, meaning that higher objects appear lighter. The graphs (G–H) present the height versus the occupied surface of the objects on typical AFM images for initial surface pressures of 20 mN/m (black dots) and 30 mN/m (open squares) for R20–24 (G) and R1–3 (H).

Compared with the pure lipid images, these protrusions are attributed to the presence of the proteins forming clusters with varying from grey to white color depending on their height relative to the background. The analysis of these images allows us to assess the variation of the height of the objects versus the surface-area occupied by the protein (Fig. 2G and H). In addition, the number of clusters and the total surface occupied were calculated (Table S1 of Supplementary material).

The image of R20–24 adsorption in DOPC/DOPS 1/1 film at an initial surface pressure of 20 mN/m (Fig. 2C) shows a heterogeneous distribution of protein clusters of variable surface-area making up 0.5% of the total surface (Table S1 in the supplementary material). When the lipid initial surface pressure is 30 mN/m, the number of these clusters is increased ten-fold and the cluster height two-fold compared to clusters at 20 mN/m (Table S1 and Fig. 2D and G), leading to a four-fold increase in the percentage of protein surface. In the latter case, some larger clusters appear with a surrounding zone devoid of protein, indicating that these large clusters are formed by the recruitment of several smaller clusters. At an initial pressure of 20 mN/m, the lipid compacity is rather low and thus could promote the insertion of proteins into the lipid film by means of hydrophobic forces. Nevertheless, the number of R20–24 clusters at this initial surface pressure of 20 mN/m is rather small and the amount of protein at the interface is very low despite its amphiphilic character. Then, it is likely that the protein interacts slightly with the lipid film and remains largely in the solution. At the higher initial surface pressure of 30 mN/m the negative charge density is higher than at 20 mN/m, which therefore favours an electrostatic interaction of the

protein with the lipid polar heads. That seems to be the case; indeed the number and the height of clusters are higher at 30 mN/m than at 20 mN/m suggesting a recruitment and a piling up of the protein at the lipid interface. As the surface occupied by R20–24 clusters is higher at 30 mN/m than at 20 mN/m, it appears that there is an electrostatic binding of the protein to the lipids without contribution of hydrophobic forces.

The image of R1–3 at the interface at an initial lipid surface pressure of 20 mN/m is shown in Fig. 2E. R1–3 is present with a 3.5-fold higher number of clusters compared to R20–24 (Table S1). Moreover, there is a very heterogeneous distribution of clusters with a highly variable surface and a low height (Fig. 2B and F). The total surface occupied by the protein is as high as 3.3% (6.6 times the surface occupied by R20–24). At an initial pressure is 30 mN/m (Fig. 2D and F), the film appears completely different from the film at 20 mN/m, with twice as many clusters occupying a smaller surface of 2.2% compared to 3.3% at 20 mN/m (Table S1). The clusters are more heterogeneous in height and surface at 30 mN/m than at 20 mN/m, in accord with the decrease in surface occupied by the protein. These changes reveal an electrostatic character at the lipid/protein binding. As a control, additional experiments with R1–3 were performed with each of the lipids alone to ensure that the binding was related to the electrostatic charge of the anionic lipid, the AFM image analysis (Table S1) showed that the number of particles is significantly lower for the DOPC monolayer compared to the DOPS monolayer and confirms the electrostatic effect.

At an initial pressure of 20 mN/m, the low lipid compacity promotes a partial insertion of R1–3 into the lipid film associated with hydrophobic interaction, and the protein spreads out over the lipid film without piling up. The insertion occurs without a regular arrangement of the protein being promoted by the lipid surface. Variations in height of the clusters at the lowest initial pressure could be due to two different processes. Firstly, protein adsorption takes place under the lipid film due to the anionic electrostatic forces of PS, while, secondly, protein insertion is promoted by hydrophobic forces. By contrast, at the high initial pressure of 30 mN/m anionic electrostatic forces prevail over hydrophobic forces, while the stronger lipid packing appears to limit the possibility of protein insertion for R1–3 as well as R20–24, leading to a piling up of the proteins. Indeed, AFM data show that for the high initial surface pressure the behaviour of both proteins seems very close. At the lower initial surface pressure R1–3 partially inserts into the monolayer while R20–24 remains only bound by electrostatic forces without insertion.

3.2.3. Orientation and conformation of proteins in interaction with lipid monolayer studied by PM-IRRAS spectroscopy

PM-IRRAS spectra were collected after injection of the protein into the sub-phase beneath the DOPC/DOPS (1:1) monolayer stabilized at 20 mN/m. Three spectra were recorded, two during the kinetic absorption and stabilization of the surface pressure and one after compression of the mixed protein/lipid monolayer up to 30 mN/m.

First of all, before injection of the proteins beneath the lipid film, a lipid spectrum was recorded at a surface pressure of 20 mN/m. This lipid monolayer spectrum is in accordance with previously published results (Fig. 3A) [27–29]. It shows a positive band around 1726 cm^{-1}, which corresponds to the C O stretching vibration (ν(C O)) of the head-group of both lipids. A very small peak at 1464 cm^{-1} can be attributed to the stretching vibration of the C—H groups of the lipid alkyl chains (ν(C—H)). A noisy signal is observed in the region between 1500 and 1600 cm^{-1}. Le Calvez et al. [30] reported that the signal of carboxylate antisymmetric band (νa(COO^-)) appears in this wavenumber range. Therefore, the perturbation observed in the lipid monolayer spectrum could be attributed to the presence of phosphatidylserine COO^- head-group, which makes up half of the lipid film.

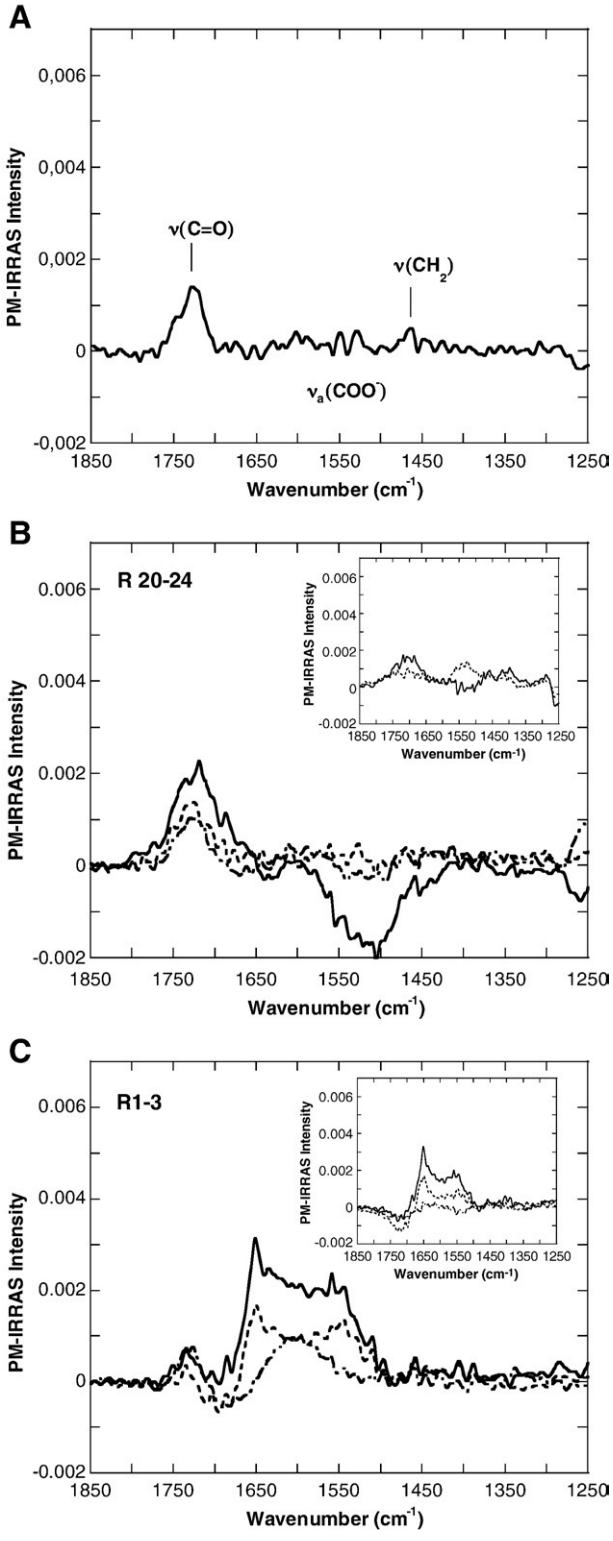

Fig 3. Representative PM-IRRAS spectra acquired during adsorption of proteins onto the lipid monolayer. The lipid film composed of DOPC/DOPS 1:1 is formed at the air/liquid interface at a surface pressure of 20 mN/m. (A) a control spectrum is recorded before protein injection beneath the lipid monolayer formed at the air/liquid interface at a surface pressure of 20 mN/m. No significant changes appear on the spectrum during compression up to 30 mN/m. (B, C) spectra are recorded during the adsorption of R20–24 and R1–3, respectively and obtained by calculating the ratio with the buffer spectrum, except in the insert where the ratio is calculated with the lipid spectrum. Spectra are acquired after the protein injection during the surface pressure increase (dash–dot–dot), during the surface pressure plateau (short dash) and after the film compression at 30 mN/m (solid line).

The NH^{3+} head-group of this lipid could give a band at 1050 cm^{-1}, but no signal is detected at this surface pressure.

Fig. 3B, C shows the spectra of the two proteins in the presence of a DOPC/DOPS monolayer.

There are no clear changes observed during the adsorption of R20–24 at the lipid/liquid interface (Fig. 3B), and no modification of the positive peak corresponding to the C O stretching vibration at about 1733 cm^{-1}. However, the intensity of this peak increases slightly, indicating that lipid packing is not modified by the protein. To eliminate the lipid signal from the protein signal, we represent the ratio of protein/lipid with respect to lipid in the insert of Fig. 3B. Very small signals are observed in the amide I and II region, meaning that the presence of the protein cannot be clearly demonstrated. However, the compression of the film up to 30 mN/m induces an enhancement of the peak located around 1733 cm^{-1}, with a shoulder at 1686 cm^{-1}, and the appearance of a negative band around 1510 cm^{-1}. The 1550 to 1500 cm^{-1} band of the COO^{-} vibration is attributed to the serine head-group in both spectra. The very large magnitude of this band leads us to propose a major reorientation of the PS head-group in contact with the protein. Moreover, the absence of any clear amide I or II bands suggests that the major part of each protein molecule remains in the sub-phase, with only a few residues being involved in binding to the serine lipid head-group. Furthermore, the intensities of the bands assigned to the acyl chain (spectra shown in the Fig. S2 A) are slightly affected by the injection of R20–24 under the lipid film suggesting few changes in the amount of lipidic matter under the infrared beam and in the hydrophobic organization of the film.

By contrast to R20–24, the injection of R1–3 clearly modifies the spectrum in the region from 1500 cm^{-1} to 1700 cm^{-1} (Fig. 3C). Three maxima are observed on the plateau (with stable surface pressure, Fig. S1), at 1733 cm^{-1}, 1651 cm^{-1} and 1553 cm^{-1}, which are attributed to the lipid carbonyl group and the protein amide I and II bands, respectively. Furthermore, the two latter are representative of the α-helical structure, indicating that the protein is clearly present at the interface, in contrast with R20–24, and that its alpha-helical structure is preserved. The C O peak intensity decreases with respect to the lipids alone, implying a reorientation of lipids at the interface. However, the carbonyl vibration is still at a high frequency which reflects the presence of a dehydrated ester group even after the protein adsorption. When the surface pressure of the mixed R1–3/lipid monolayer is increased to 30 mN/m, the three peaks are maintained at the same wavenumber and their intensity increases. The C O peak intensity recovers its initial intensity, which is representative of the lipid packing observed at 20 mN/m before protein injection.

Amide I and amide II peaks increase in the same proportion. Therefore, the amount of R1–3 at the interface increases without any change in the protein helical content. RI/II rises from 1 to 1.55, which reflects a minor change from 40° to 45° in the average angle of helices with respect to the monolayer normal. Consequently, we may conclude that the film is compressed without expulsion of the protein and that the lipids and the protein are stabilized at the interface even at the highest surface pressure, indicating an involvement of strong interactions in the binding of R1–3 to lipids. In the region of the C–H stretch of acyl chains (wavenumber range from 3000 to 2600 cm^{-1}, Fig. S2 B), the presence of R1–3 causes a disappearance of two bands. In accordance with the previous results, the acyl chains are clearly affected by the protein R1–3 suggesting the insertion of the protein in the hydrophobic part of the film and its stabilization during compression.

4. Discussion

The present work is focused on the properties of two sub-domains of the dystrophin central domain with respect to an anionic lipid monolayer. R1–3 and R20–24 are composed of three and five spectrin-like repeats respectively. The two proteins are stable and soluble in solution (non-aggregation), and their secondary structure is composed at least of 75% of α-helices [12]. Each repeat is structured in a triple helical coiled-coil and the multirepeat proteins are formed of chained-up repeats [31]. The surface pressure-measurements at the air/liquid interface show that the pure absorbed proteins exhibit a high affinity for the interface where they are able to form stable interfacial films. To account for the high surface pressure observed with the two proteins, we should bear in mind that high surface pressure is related to a high degree of lateral protein packing and a large area occupied by the protein at the air/liquid interface. Therefore, it is clear that the two proteins display an amphiphilic character. A similar conclusion was previously proposed for a construct of R2 with the same plateau value of about 20 mN/m observed at the air/liquid interface [4]. In addition, we show here that longer proteins such as R1–3 and R20–24 display similar properties at the interface. PM-IRRAS spectra show a high α-helix content with no strong structural changes appearing at the air/liquid interfaces, indicating that the proteins maintain their helical secondary structure [16].

From these results, it appears that this strong interfacial activity without α-helical unfolding could be a characteristic feature of all spectrin-like repeats of dystrophin, as previously shown for a single repeat [4]. Nevertheless, there could be some differences between the repeats, including the requirement of a highly hydrated environment for R20–24.

After this preliminary study of the behaviour of the two proteins at the air/liquid interface, we then applied the membrane model to investigate the interactions of the proteins with lipids.

The AFM image analyses clearly show an effect of the lipid initial surface pressure on the number of protein particles observed at the interface as well as the total surface occupied by the protein. Although the lipids stay in a liquid-expanded state both proteins are more present in the anionic lipid film when the initial surface pressure is 30 mN/m compared to 20 mN/m. The value of the higher surface pressure is chosen from the literature as corresponding to a reasonable estimate of the surface pressure in biological membranes [32–35]. However, although R20–24 is an amphiphilic protein, it displays a poor ability to bind strongly with the anionic lipid monolayer as shown by AFM and PM-IRRAS. This is in line with previous results showing that R20–24 is not able to form stable lipid–protein complexes and that the Trp environment in the protein is not modified by the presence of anionic vesicles [12]. These latter authors [12] used the highly curved model of membrane of small unilamellar vesicles, while, in the present study, we investigate planar geometry with phospholipid monolayers at two surface pressures, thus making up a large range of studied situations. All together, these observations lead us to conclude that the R20–24 sub-domain of the dystrophin rod interacts only very weakly with membrane phospholipids by means of a few electrostatic forces. The main part of each R20–24 molecule remains in the sub-phase. Then we could hypothesize that this part is free to interact with intracellular molecules.

In the case of R1–3 at the low surface pressure of 20 mN/m, hydrophobic interactions with lipids facilitate a partial insertion of the protein in the monolayer and promote a lateral interaction between close protein molecules, thus explaining the large surface-area occupied by R1–3. By contrast, at the high surface pressure of 30 mN/m, the proximity of anionic head-group precludes the spreading out of each protein molecule relative to its neighbours, and instead favours their piling up. In conclusion, R1–3 clearly shows a preference for the lipid/liquid interface, which can facilitate hydrophobic interactions needed for the insertion. Very interestingly, the insertion as well as the piling up does not induce unfolding of the α-helices.

In addition, even though it is very difficult to interpret the angular data as the protein is made up of nine helices, the helices form bundles

that could be assigned to a single global elongated macromolecule. The angle with respect to the normal at the monolayer ranges from 40 to 45°, depending on the surface pressure. This angle is smaller compared to the angle of 61° observed for the protein at the air/liquid interface. This is highly indicative of a preference of the protein for the lipid environment, in agreement with its high interfacial activity.

R1–3 represents a true sub-domain of the dystrophin rod domain delineated by two hinges. It could be an essential domain in the stabilization of protein–membrane interaction, and could be biologically highly relevant [36]. Dystrophin mechanically anchors cytoplasmic γ-actin filaments of the cortical cytoskeleton to the sarcolemma via a direct interaction of the N-terminal actin-binding domain of dystrophin with γ-actin [3]. This actin-binding domain is separated from the R1–3 rod sub-domain only by a hinge. Thus, it is tempting to hypothesize that R1–3 binding to membrane lipids could strongly help to localize γ-actin close to the sarcolemma. On the C-terminal end of the rod domain, the R20–24 sub-domain could even provide a weak electrostatic binding to the membrane, thus reinforcing the dystrophin WW domain interaction with the membrane protein β-dystroglycan by maintaining dystrophin near the membrane layer [36]. On the other hand, a recent study based on microtubule cosedimentation assay suggests that the repeat 24 with the first third part of WW domain is involved in binding of microtubules [37]. Then, if only few residues of R20–24 interact with anionic lipids of the membrane, the other ones could interact with components of the cellular cytoskeleton such as microtubules.

In addition, in dystrophin-deficient muscles, it is striking that the sarcolemma ruptures very frequently. Moreover, a higher susceptibility to eccentric contractions is observed, which leads to calcium entry into the damaged cells and leakage of the cellular content such as creatine kinase [7,38]. Accordingly, immobilization of dystrophin-deficient muscles by knocking out of the acetylcholinesterase receptor gene is accompanied by reduced signs of dystrophy [39]. This provides clear evidence that dystrophin is involved in the resistance of sarcolemmal membrane against stress induced by the contraction–relaxation cycles of active muscle. As shown in the present study, the R1–3 sub-domain of the dystrophin rod could play a central role in such a resistance, and could be partly inserted into the monolayer at low surface pressure through hydrophobic forces and under compression could remained tightly attached to the monolayer through electrostatic forces. This model of modulation of the monolayer by surface pressure is close to the situation that takes place in the muscle at work, i.e. dynamic and cyclic changes of membrane tensile strength encountered by the muscle membrane during contraction (higher surface pressure) and relaxation (lower surface pressure). Therefore, dystrophin sub-domain R1–3 could provide the phospholipid membrane with a solid support that is essential for maintaining membrane cohesion [40,41]. Finally, in support of a role of R1–3 binding to membrane lipids, it is known that truncated dystrophins lacking this region are less efficient to rescue the normal phenotype of the dystrophin-deficient *mdx* mouse [42,43], compared to constructs containing these repeats, showing that this part of the rod domain is essential for a normal function of dystrophin.

Acknowledgements

This work was supported in part by the “Association Française contre les Myopathies” (AFM). SL was a recipient of a grant from the “Conseil Régional de Bretagne” (PRIR 1351). The authors wish to thank S. Pezennec for valuable discussions. M.S.N. Carpenter post-edited the English style.

Appendix A. Supplementary data

Supplementary data associated with this article can be found, in the online version, at doi:10.1016/j.bbamem.2010.04.005.

References

[1] M. Koenig, A.P. Monaco, L.M. Kunkel, The complete sequence of dystrophin predicts a rod-shaped cytoskeletal protein, Cell 53 (1988) 219–226.
[2] K. Ohlendieck, K. Campbell, Dystrophin constitutes 5% of membrane cytoskeleton in skeletal muscle, FEBS Lett. 283 (1991) 30–234.
[3] J.M. Ervasti, Dystrophin, its interactions with other proteins, and implications for muscular dystrophy, Biochim. Biophys. Acta 1772 (2007) 108–117.
[4] C. DeWolf, P. McCauley, A.F. Sikorski, C.P. Winlove, A.I. Bailey, E. Kahana, J.C. Pinder, W.B. Gratzer, Interaction of dystrophin fragments with model membranes, Biophys. J. 72 (1997) 2599–2604.
[5] E. Le Rumeur, Y. Fichou, S. Pottier, F. Gaboriau, C. Rondeau-Mouro, M. Vincent, J. Gallay, A. Bondon, Interaction of dystrophin rod domain with membrane phospholipids: evidence of a close proximity between tryptophan residues and lipids, J. Biol. Chem. 278 (2003) 5993–6001.
[6] S. Legardinier, C. Raguénès-Nicol, C. Tascon, C. Rocher, S. Hardy, J.F. Hubert, E. Le Rumeur, Mapping of the lipid-binding and stability properties of the central rod domain of human dystrophin, J. Mol. Biol. 389 (2009) 546–558.
[7] B.J. Petrof, J.B. Shrager, H.H. Stedmann, A.M. Kelly, H.L. Sweeney, Dystrophin protects the sarcolemma from stresses developed during muscle contraction, Proc. Natl. Acad. Sci. U. S. A. 90 (1993) 3710–3714.
[8] V. Straub, J.A. Rafael, J.S. Chamberlain, K.P. Campbell, Animal models for muscular dystrophy show different patterns of sarcolemmal disruption, J. Cell Biol. 139 (1997) 375–385.
[9] F. Nguyen, Y. Chérel, L. Guigand, I. Goubault-Leroux, M. Wyers, Muscle lesions associated with dystrophin deficiency in neonatal golden retriever puppies, J. Comp. Pathol. 126 (2002) 100–108.
[10] M. Koenig, L.M. Kunkel, Detailed analysis of the repeat domain of dystrophin reveals four potential hinge segments that may confer flexibility, J. Biol. Chem. 265 (1990) 4560–4566.
[11] S. Winder, T. Gibson, J. Kendrick-Jones, Dystrophin and utrophin: the missing links! FEBS Lett. 369 (1995) 27–33.
[12] S. Legardinier, J.-F. Hubert, O. Le Bihan, C. Tascon, C. Rocher, C. Raguénès-Nicol, A. Bondon, S. Hardy, E. Le Test, Sub-domains of the dystrophin rod domain display contrasting lipid-binding and stability properties, Biochim. Biophys. Acta 1784 (2008) 672–682.
[13] H. Brockman, Lipid monolayers: why use half a membrane to characterize protein–membrane interactions? Curr. Opin. Struct. Biol. 9 (1999) 438–443.
[14] W. Diakowski, A. Sikorski, Brain spectrin exerts much stronger effect on anionic phospholipid monolayers than erythroid spectrin, Biochim. Biophys. Acta 1564 (2002) 403–411.
[15] M. Grzybek, A. Chorzalska, E. Bok, A. Hryniewicz-Jankowska, A. Czogalla, W. Diakowski, A.F. Sikorski, Spectrin–phospholipid interactions. Existence of multiple kinds of binding sites? Chem. Phys. Lipids 141 (2006) 133–141.
[16] D. Blaudez, T. Buffeteau, J.-C. Cornut, B. Desbat, N. Escafre, M. Pézolet, J.-M. Turlet, Polarization-modulated FT-IR spectroscopy of a spread monolayer at the air/water interface, Appl. Spectrosc. 47 (1993) 869–874.
[17] E. Bellet-Amalric, D. Blaudez, B. Desbat, F. Graner, F. Gauthier, A. Renault, Interaction of the third helix of Antennapedia homeodomain and a phospholipid monolayer, studied by ellipsometry and PM-IRRAS at the air–water interface, Biochim. Biophys. Acta 1467 (2000) 131–143.
[18] V. Vié, N. Van Mau, L. Chaloin, E. Lesniewska, C. Le Grimellec, F. Heitz, Detection of peptide–lipid interactions in mixed monolayers, using isotherms, atomic force microscopy, and fourier transform infrared analyses, Biophys. J. 78 (2000) (2000) 846–856.
[19] L. Dubreil, V. Vie, S. Beaufils, D. Marion, A. Renault, Aggregation of puroindoline in phospholipid monolayers spread at the air–liquid interface, Biophys. J. 85 (2003) 2650–2660.
[20] C. Bottier, J. Gean, B. Desbat, A. Renault, D. Marion, V. Vie, Structure and orientation of puroindolines into wheat galactolipid monolayers, Langmuir 24 (2008) 10901–10909.
[21] D. Blaudez, J.-M. Turlet, J. Dufourcq, D. Bard, T. Buffeteau, B. Desbat, Investigations at the air/water interface using polarization modulation IR spectroscopy, J. Chem. Soc. Faraday Trans. 92 (1996) 525–530.
[22] S. Castano, B. Desbat, M. Laguerre, J. Dufourcq, Structure, orientation and affinity for interfaces and lipids of ideally amphipathic lytic LiKj(i = 2j) peptides, Biochim. Biophys. Acta 1416 (1999) 176–194.
[23] T. Buffeteau, E.L. Calvez, S. Castano, B. Desbat, D. Blaudez, J. Dufourcq, Anisotropic optical constants of α-helix and β-sheet secondary structures in the infrared, J. Phys. Chem. B 104 (2000) 4537–4544.
[24] H. Lavoie, B. Desbat, D. Vaknin, C. Salesse, Structure of rhodopsin in monolayers at the air–water interface: a PM-IRRAS and X-Ray Reflectivity study, Biochemistry 41 (2002) 13424–13434.
[25] F. Picard, T. Buffeteau, B. Desbat, M. Auger, M. Pezolet, Quantitative orientation measurements in thin lipid films by attenuated total reflection infrared spectroscopy, Biophys. J. 76 (1999) 539–551.
[26] F. Ronzon, B. Desbat, J.P. Chauvet, B. Roux, Behavior of a GPI-anchored protein in phospholipid monolayers at the air–water interface, Biochim. Biophys. Acta 1560 (2002) 1–13.
[27] I. Estrela-Lopis, G. Brezesinski, H. Möhwald, Dipalmitoyl phosphatidylcholine/phospholipase D interactions investigated with polarization-modulated infrared reflection absorption spectroscopy, Biophys. J. 80 (2001) 749–754.
[28] S. Castano, D. Blaudez, B. Desbat, J. Dufourcq, H. Wroblewski, Secondary structure of spiralin in solution, at the air/water interface, and in interaction with lipid monolayers, Biochim. Biophys. Acta 1562 (2002) (2002) 45–56.
[29] J. Saccani, S. Castano, B. Desbat, D. Blaudez, A phospholipid bilayer supported under a polymerized Langmuir film, Biophys. J. 85 (2003) 3781–3787.

[30] E. Le Calvez, D. Blaudez, T. Buffeteau, B. Desbat, Effect of cations on the dissociation of arachidonic acid monolayers on water studied by polarization-modulated infrared reflection–absorption spectroscopy, Langmuir 17 (2001) 670–674.
[31] R. Calvert, E. Kahana, W.B. Gratzer, Stability of the dystrophin rod domain fold: evidence for nested repeating units, Biophys. J. 71 (1996) 1605–1610.
[32] M.C. Phillips, R.M. Williams, D. Chapman, On the nature of hydrocarbon chain motions in lipid liquid crystals, Chem. Phys. Lipids 3 (1969) 234–244.
[33] R.A. Demel, W.S. Geurts van Kessel, R.F. Zwaal, B. Roelofsen, L.L. van Deenen, Relation between various phospholipase actions on human red cell membranes and the interfacial phospholipid pressure in monolayers, Biochim. Biophys. Acta 406 (1975) 97–107.
[34] J.F. Nagle, Theory of lipid monolayer and bilayer phase transitions: effect of headgroup interactions, J. Membr. Biol. 27 (1976) 233–250.
[35] A. Blume, A comparative study of the phase transitions of phospholipid bilayers and monolayers, Biochim. Biophys. Acta 557 (1979) 32–44.
[36] G.B. Banks, J.S. Chamberlain, The value of mammalian models for Duchenne muscular dystrophy in developing therapeutic strategies, Curr. Top. Dev. Biol. 84 (2008) 431–453.
[37] K.W. Prins, J.L. Humston, A. Mehta, V. Tate, E. Ralston, J.M. Ervasti, Dystrophin is a microtubule-associated protein, J. Cell Biol. 186 (2009) 363–369.
[38] N. Deconinck, B. Dan, Pathophysiology of Duchenne muscular dystrophy: current hypotheses, Pediatr. Neurol. 36 (2007) 1–7.
[39] C. Etard, M. Behra, R. Ertzer, N. Fischer, S. Jesuthasan, P. Blader, R. Geisler, U. Strahle, Mutation in the delta-subunit of the nAChR suppresses the muscle defects caused by lack of Dystrophin, Dev. Dyn. 234 (2005) 1016–1025.
[40] O. Hamill, B. Martinac, Molecular basis of mechanotransduction in living cells, Physiol. Rev. 81 (2001) 685–740.
[41] M.P. Sheetz, J.E. Sable, H.G. Dobereiner, Continuous membrane-cytoskeleton adhesion requires continuous accommodation to lipid and cytoskeleton dynamics, Annu. Rev. Biophys. Biomol. Struct. 35 (2006) 417–434.
[42] S.Q. Harper, M.A. Hauser, C. DelloRusso, D. Duan, R.W. Crawford, S.F. Phelps, H.A. Harper, A.S. Robinson, J.F. Engelhardt, S.V. Brooks, J.S. Chamberlain, Modular flexibility of dystrophin: implications for gene therapy of Duchenne muscular dystrophy, Nature Med. 8 (2002) 253–261.
[43] M. Liu, Y. Yue, S. Harper, R. Grange, J. Chamberlain, D. Duan, Adeno-associated virus-mediated microdystrophin expression protects young mdx muscle from contraction-induced injury, Mol. Ther. 11 (2005) 245–256.